

Received April 23, 2020, accepted May 17, 2020, date of publication May 20, 2020, date of current version June 3, 2020.

Digital Object Identifier 10.1109/ACCESS.2020.2996020

# The Design of a Reconfigurable Slot Antenna Printed on Glass for Wearable Applications

ERDEM CIL AND SEMA DUMANLI<sup>1</sup>, (Member, IEEE)

Electrical and Electronics Engineering Department, Bogazici University, 34342 Istanbul, Turkey

Corresponding author: Sema Dumanli (sema.dumanli@boun.edu.tr)

This work was supported by the Bogazici University Research Fund under Grant 14543.

**ABSTRACT** A novel pattern and polarization reconfigurable wearable slot antenna suitable for smart glasses is proposed. The antenna is designed and fabricated on glass and reconfiguration is realized using four PIN diodes. It operates in the 2.4 GHz Industrial, Scientific and Medical Band. It consists of an equilateral L-shaped slot fed by a single coplanar waveguide feed. The slot is manipulated with switches to generate two modes of operation. Each mode corresponds to one of the two states of the switches which result in different L-shaped slots with unequal legs creating patterns that are polarized in perpendicular to each other. The antenna has been shown to perform well near the human body using numerical and physical phantoms. The correlation between the two modes is calculated to be less than 0.04 with 41% and 56% on-body efficiency for each mode. The Specific Absorption Rate is shown to be well below the limit specified in the European Standards through simulations.

**INDEX TERMS** Antenna radiation pattern, glass, slot antenna, wireless body sensor network.

## I. INTRODUCTION

Remote monitoring of people's health is one of the main goals that the Internet of Health Things (IoHT) focuses on [1]. Advancements in technology have led to the development of small and smart electronic devices that can be placed on or inside the human body [2]. These wearable and implantable devices form the basis of the IoHT and continuously monitor diverse physiological parameters of healthy individuals or patients. Although the design of such devices is highly multidisciplinary, it can be argued that the careful design of the antenna is one of the most important aspects for an optimum solution.

The design of an antenna operating near the human body has its unique challenges. Firstly, the antenna is located near lossy human tissues which leads to detuning effects as well as efficiency degradation due to near field losses [3]. Moreover, these effects are dependent on the body composition of that particular individual and near which part of the body the antenna is located. In addition, the mobility of the human body leads to dynamic channels requiring changing radiation patterns to ensure the best link quality as the person moves around [4]. Reconfigurable antennas can be utilized to mitigate these challenges [5].

The associate editor coordinating the review of this manuscript and approving it for publication was Lorenzo Mucchi<sup>1</sup>.

Reconfigurable antennas are antennas that are able to manipulate their radiation characteristics by redistributing the current on the radiating aperture of the antenna. Thus, their radiation characteristics can be modified according to the altering environmental conditions [6], [7]. The reconfiguration of the radiation characteristics can be performed in four different forms [8]. The reconfiguration can take place in operating frequency [9]–[14], polarization [15]–[18], radiation pattern [19]–[27] or any combination of these characteristics [28]–[30].

Radiation pattern reconfiguration can be implemented to increase the probability of getting a reliable link over time. The pattern can be switched between predefined patterns to find the one supporting the best link quality as the human body moves and the direction of arrival changes [4]. Here, a novel pattern reconfigurable wearable slot antenna is proposed. The slot antenna is preferred due to their robustness against detuning effects. Note that since the size is restricted in wearable applications, utilization of arrays is not an option. In the literature, a number of reconfigurable slot antennas have been proposed [17], [18], [21], [22], [27], [29]. Among these, [17] and [21] differ from the existing design by the fact that they consist of multiple ports and the reconfiguration is intended by port selection. [18], [22], [27] and [29] successfully realize reconfiguration, although they are not intended and hence not suitable for wearable applications.

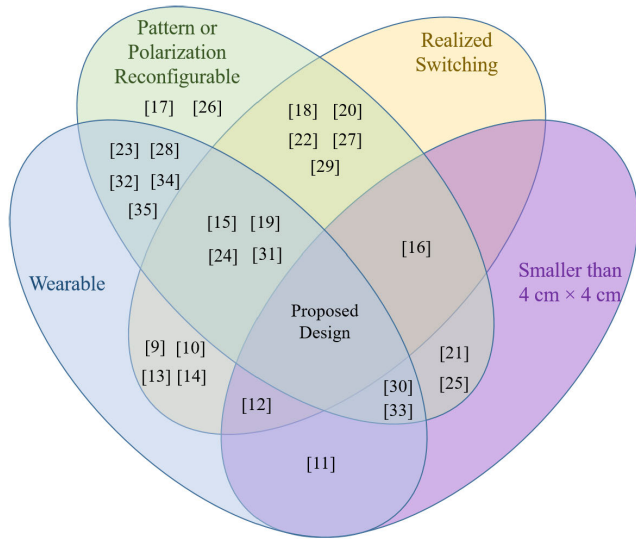
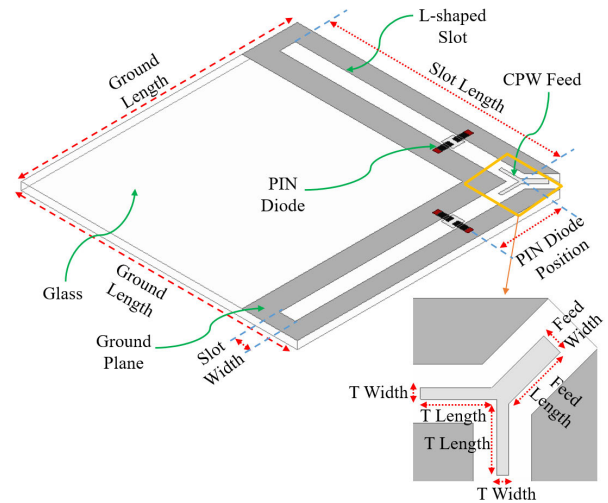


**FIGURE 1. A comparison between the proposed antenna and related reconfigurable antennas in the literature.**

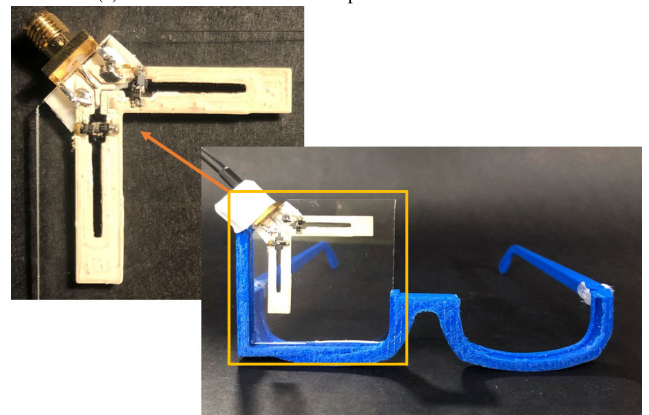
Specifically, [22] and [29] have thick profiles of 7.2 mm (2.3 - 2.4 GHz) and 4.5 mm (1.8 - 2.1 GHz), respectively, and [18] and [27] have large electrical sizes of  $0.69\lambda_0 \times 0.56\lambda_0$  and  $0.83\lambda_0 \times 0.83\lambda_0$ , respectively.

Here, an equilateral L-shaped slot that is switched between two operation modes is proposed. Two states of switches lead to two different L-shaped slots with unequal legs that are excited by the same coplanar waveguide (CPW) feed. Since the L-shaped slots are oriented in different directions, two patterns that are polarized in perpendicular to each other are created. The overall dimensions are 35 mm × 35 mm × 1 mm. The design mainly differs from the state of the art in two ways. First, the reconfiguration of the pattern is not achieved through manipulating the feedline or exciting new elements that accompany the main radiating aperture, but through creating two operation modes from a single slot. Second, glass is used as the substrate of the proposed antenna; whereas conventionally, along with standard substrates such as FR4-Epoxy [19], [23], [24], flexible substrates [28], [31]–[34] are exploited in wearable pattern reconfigurable antennas. To the authors’ knowledge, there is no pattern-reconfigurable wearable antenna designed on glass. The utilization of glass as the substrate makes the proposed antenna preferable for the applications where visibility through the wearable device is required such as smart glasses. A comparison between the proposed antenna and related reconfigurable antennas in the literature is provided in Fig. 1. Note that an earlier version of that antenna was presented by the authors in [35]. This improved version is drastically different in terms of both the structure and the feeding mechanism as well as the substrate used.

This paper is organized as follows. In section II, the design process of the antenna is explained and the antenna model is described. In section III, the process for the formation of the physical head phantom used in the measurements is



(a) The antenna model and the parameterized dimensions



(b) The prototype of the antenna inserted in a 3D printed glasses frame

**FIGURE 2. The proposed model and the prototype of the antenna.**

introduced. In section IV, the simulation and measurement results are given and interpreted. Section V concludes the work.

## II. ANTENNA MODEL AND PROTOTYPE

The proposed antenna is designed to operate in the 2.4 GHz Industrial, Scientific and Medical (ISM) band on glass with a relative permittivity of 8.5 and a thickness of 1 mm as can be seen in Fig. 2. The overall dimensions of the substrate are chosen to be 35 mm × 35 mm appropriate for standard glasses. The antenna is placed along the two edges of the substrate so that the visibility through the glass is not obstructed. The equilateral L-shaped slot consists of a horizontal and a vertical part. The feed is located at the corner. The location of the feed with respect to the radiating slot is critical in tuning the input impedance of the antenna as well as the length of the T-junction arms. The radiation pattern of the antenna is switched between two different modes, horizontal mode or vertical mode, using PIN diodes. The horizontal mode corresponds to the L-shaped slot with longer horizontal section. It creates dominantly a vertical polarization. Note that the length of the shorter vertical section will affect the

position of the feed with respect to the slot and hence the input impedance of the antenna, as mentioned before. The vertical mode corresponds to the L-shaped slot with longer vertical section creating a horizontal polarization.

The length of L-shaped slots and the location of the feed are analytically calculated with a narrow slot assumption. The results of the analytic calculation will later be used as the initial value of the slot length and the position of the feed in the numerical optimization. Following the initial narrow slot assumption, the width of the slot is taken to be much smaller than the guided wavelength,  $\lambda_{guided}$ , making the  $TE_{10}$  the dominant mode and enabling the calculation of the slot length using (1) [36]. The guided wavelength can be calculated from the free space wavelength,  $\lambda_0$ , as in (2). An effective permittivity,  $\epsilon_{eff}$ , must be used here due to the fact that the electric field created by the antenna is contained both in air and in the dielectric material. It can be calculated by means of a filling factor,  $ff$ , as in (3). The filling factor here is taken to be 0.5 which is the typical value for CPW. Hence, the effective permittivity for glass is calculated to be 4.75. The guided wavelength is calculated to be 56.18 mm at 2.45 GHz; hence, the length of the slot should be 28.09 mm.

$$L_{TE10} = \frac{\lambda_{guided}}{2} \quad (1)$$

$$\lambda_{guided} = \frac{\lambda_0}{\sqrt{\epsilon_{eff}}} \quad (2)$$

$$\epsilon_{eff} = \epsilon_R * ff + (1 - ff) \quad (3)$$

As for the calculation of the feeding location, the slot can be considered as the dual of a half-wave dipole. This enables the calculation of the radiation resistance of the slot,  $R_{slot}$ , by duality as in (4) [37]. Given that the radiation resistance of the complementary dipole,  $R_{dipole}$ , is 73  $\Omega$  and the intrinsic impedance of the free space,  $Z_0$ , is 377  $\Omega$ , the radiation resistance of the slot is calculated to be 487  $\Omega$ . Although this is a large value, the matching can be achieved by using an off center feeding. For a 50  $\Omega$  coaxial cable, the offset of the feeding point from the center of the slot,  $L_{offset}$ , can be calculated using (5) [38], which equals 11.24 mm when the guided wavelength is 56.18 mm.

$$R_{slot} = \frac{Z_0^2}{4R_{dipole}} \quad (4)$$

$$L_{offset} = \frac{\lambda_{guided}}{5} \quad (5)$$

Beginning with the calculated values, the length of the L-shaped slots, the location and the dimensions of the feed line are optimized through numerical analysis using ANSYS High Frequency Structure Simulator (HFSS) [39]. The point that is of great importance here is that the design is symmetrical with respect to the diagonal of the antenna. This symmetry ensures that when the performance of the antenna is optimized at 2.45 GHz for one of the modes, its performance for the other mode is optimized as well since two modes only differ in the orientation of the L-shaped slots. The final values of the dimensions are tabulated in Table 1. The antenna is

TABLE 1. The optimized values of the parameterized dimensions.

Parameters	Final Values (mm)
Slot Length	24.3
Slot Width	1.6
PIN Diode Position	7.8
Ground Length	35
Feed Length	3.5
Feed Width	1.2
T Length	1.7
T Width	0.7

prototyped using Voltera V-One [40]. Conductive ink with a conductivity of 1052632 S/m at DC is dispensed on a glass substrate with an accuracy of 0.2 mm and cured at 200  $^{\circ}$ C as seen in Fig 2(b).

### III. MEASUREMENT SET-UP

Since the antenna is designed to be implemented in smart glasses, it will always be operating in close proximity of a human head. Therefore, it is essential to evaluate the detuning effects of the human body on the operation of the antenna. For this purpose, the antenna is tested on a two-layer phantom and on human subjects. The two-layer phantom as visioned in Fig. 3 consists of a 3D printed container and semi-solid tissue mimicking mixtures. The container is made of PLA and 10 cm  $\times$  10 cm  $\times$  10 cm in size. It has a special compartment for the eye phantom to be located and a planar clamp to fix the antenna and the cabling. Two different mixtures that mimic the electrical properties of the eye tissue and the muscle tissue are prepared using water, agar, gelatine, corn flour, sodium azide, sodium chloride, and propylene glycol [41]. At 2.45 GHz, the electrical properties of the eye tissue and the muscle tissue are given as  $\epsilon_R = 53$ ,  $\sigma = 2.2$  S/m [41] and  $\epsilon_R = 52.7$ ,  $\sigma = 1.74$  S/m [42], respectively. The quantities of ingredients used to prepare the mixtures are tabulated in Table 2. In order to validate the relative permittivity and the conductivity values of prepared mixtures, the open-ended coaxial probe method explained in [43] is exploited. A 9 cm RG402 coaxial cable is used as the open-ended coaxial probe. A code implementing the mathematical procedure summarized in [43] is developed. The measured values are  $\epsilon_R = 48$  and  $\sigma = 2.5$  S/m for the eye tissue and  $\epsilon_R = 48.5$  and  $\sigma = 2$  S/m for the muscle tissue. The eye mimicking mixture is pumped into a circular latex balloon with 50 mm diameter and placed at its special compartment. The container is then filled with the muscle mimicking mixture as seen in Fig. 3(b). The measurements on the human subjects are taken using a 3D printed glasses frame as in Fig. 3(c). The corresponding simulations are conducted on ANSYS human body phantom, Male-4mm accuracy as seen in Fig. 3(d).

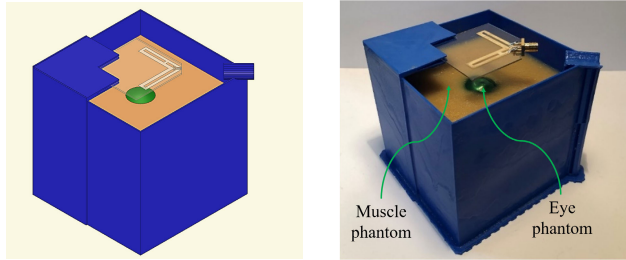
## IV. RESULTS AND DISCUSSION

### A. RESULTS IN AIR

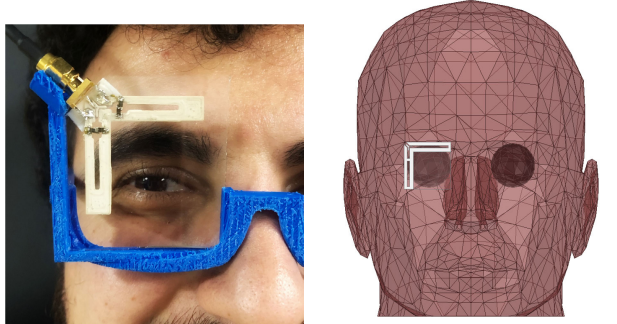
The simulated and measured return loss in air for the horizontal and vertical mode is shown in Fig. 4. It is observed that the simulated frequency responses of the horizontal and

**TABLE 2.** The quantities of ingredients used per 100 g mixture.

Ingredient	Eye Tissue (g)	Muscle Tissue (g)
Distilled Water	75.62	75.62
Corn Flour	4.72	4.72
Gelatine	14.52	15.35
Agar	3.02	3.02
Sodium Azide	0.3	0.3
Propylene Glycol	0.6	0.6
Sodium Chloride	1.21	0.38



(a) The numeric version of the two-layer phantom (b) The physical version of the two-layer phantom



(c) The antenna worn by a human (d) ANSYS human body phantom subject

**FIGURE 3.** Different versions of the measurement setups used to evaluate the operation of the antenna near the human body and their numerical counterparts.

vertical modes are identical to each other as expected due to the symmetry of the structure. It can also be seen from Fig. 4 that for both modes of operation, the measured and simulated reflection coefficients agree. The center frequency estimated by numerical analysis is 2.47 GHz, and the measured center frequency is the same for the horizontal mode and 2.48 GHz for the vertical mode. The disagreement is within the limits of manufacturing accuracy.

Fig. 5 shows the simulated 3D radiation patterns of the operation modes in air along with the corresponding 2D cross sections at  $\phi = 0^\circ$  and  $\phi = 90^\circ$ . It can be observed that the patterns in both modes are omnidirectional and their polarizations are perpendicular to each other. The null of the pattern is at  $\theta = 90^\circ, \phi = -106^\circ$  for the horizontal mode, whereas it is at  $\theta = 90^\circ, \phi = 18^\circ$  for the vertical mode. The maximum gains are 1.9 dBi at  $\theta = 152^\circ, \phi = 8^\circ$  for the horizontal mode and 1.6 dBi at  $\theta = 148^\circ, \phi = -90^\circ$  for the vertical mode. Fig. 6 shows the measured normalized 3D far-field radiation pattern of the horizontal mode in air along with the corresponding 2D cross sections at  $\phi = 0^\circ$

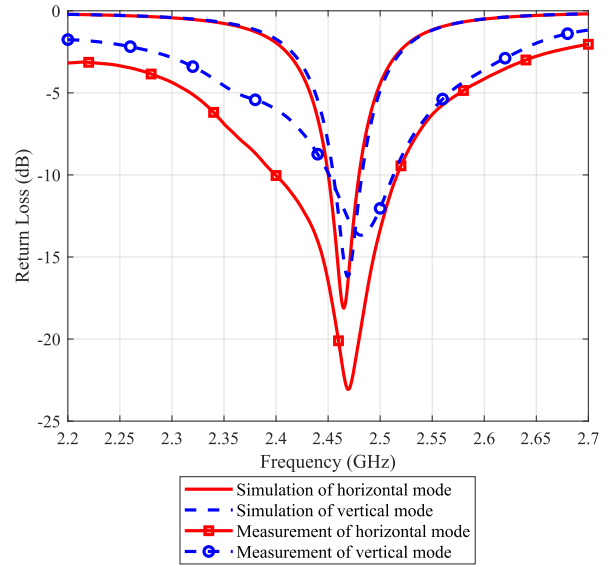


**FIGURE 4.** Simulated and measured frequency responses in air. Horizontal mode:  $-18.1$  dB at 2.47 GHz in simulation and  $-23$  dB at 2.47 GHz in measurement. Vertical mode:  $-16.2$  dB at 2.47 GHz in simulation and  $-13.7$  dB at 2.48 GHz in measurement.

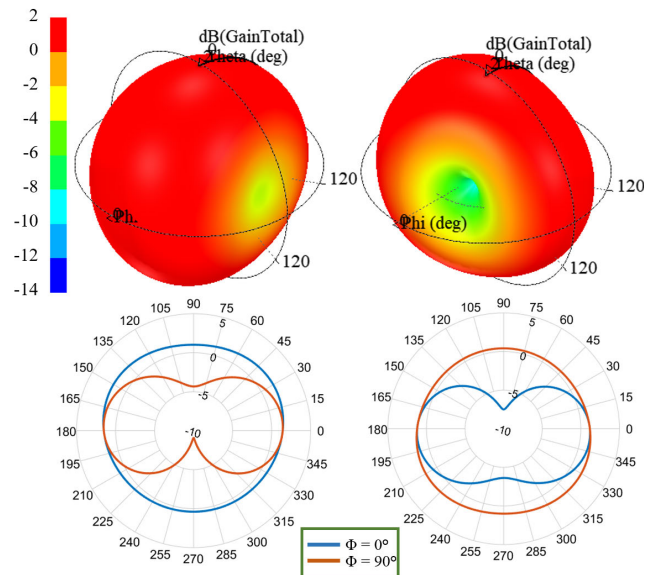


**FIGURE 5.** Simulated 3D radiation patterns and the corresponding 2D cross sections at  $\phi = 0^\circ$  and  $\phi = 90^\circ$  of the horizontal (left) and vertical (right) mode in air with maximum gains of 1.9 dBi and 1.6 dBi, respectively.

and  $\phi = 90^\circ$  using a planar near-field setup. The pattern is expected to be symmetrical with respect to xy-plane. Good agreement can be observed. The radiation efficiency for the horizontal mode is measured as 41% using the same planar setup.

**B. ON-BODY PERFORMANCE**

In order to analyze the realistic performance of the antenna, it is tested on numerical and physical phantoms as well as human subjects as described in Section III. Fig.7 shows the simulated and measured return loss graphs on the two-layer

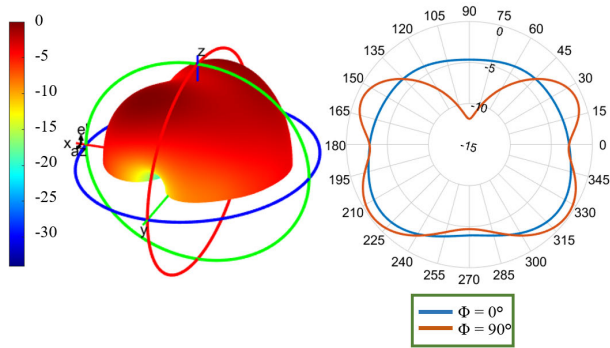


**FIGURE 6.** Measured normalized radiation pattern and the corresponding 2D cross sections at  $\phi = 0^\circ$  and  $\phi = 90^\circ$  of the horizontal mode in air.

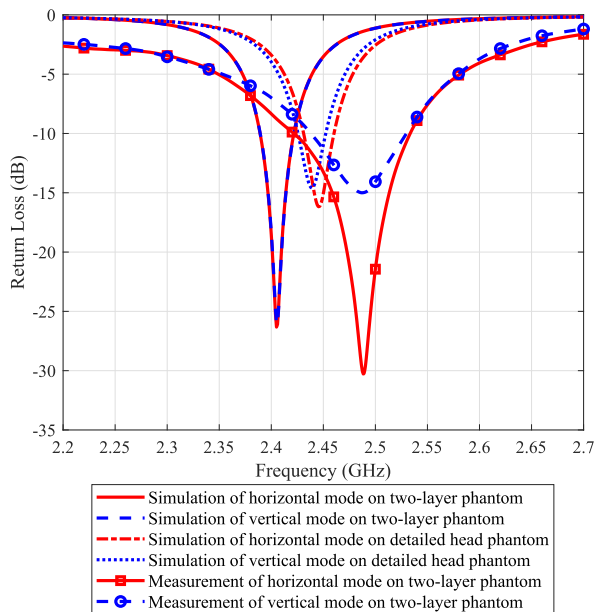


**FIGURE 7.** Simulated and measured frequency responses on two-layer phantom and simulated frequency responses on the ANSYS human body phantom. Horizontal mode:  $-26.1$  dB at  $2.41$  GHz in simulation on two-layer phantom,  $-16$  dB at  $2.44$  GHz in simulation on ANSYS human body phantom, and  $-30.3$  dB at  $2.49$  GHz in measurement on two-layer phantom. Vertical mode:  $-26.3$  dB at  $2.41$  GHz in simulation on two-layer phantom,  $-14.4$  dB at  $2.44$  GHz in simulation on ANSYS human body phantom, and  $-15$  dB at  $2.49$  GHz in measurement on two-layer phantom.

phantom as well as the simulations on the Ansys male phantom. It can be noticed that the estimated center frequency is lower than the actual measured center frequency. This trend prevails for measurements on human subjects. Hence, the reason behind this is predicted to be the inaccuracies in the electrical and physical properties of human tissues used for the simulations. Although the models could not be improved, the effect is found to be predictable which can be modeled at the earlier stages of the design. The fact that the simulated results for the two-layer phantom and the Ansys male phantom differ gives an indication that the final measurements should be taken on human subjects. Note that the return loss is greater than 10 dB for all cases.

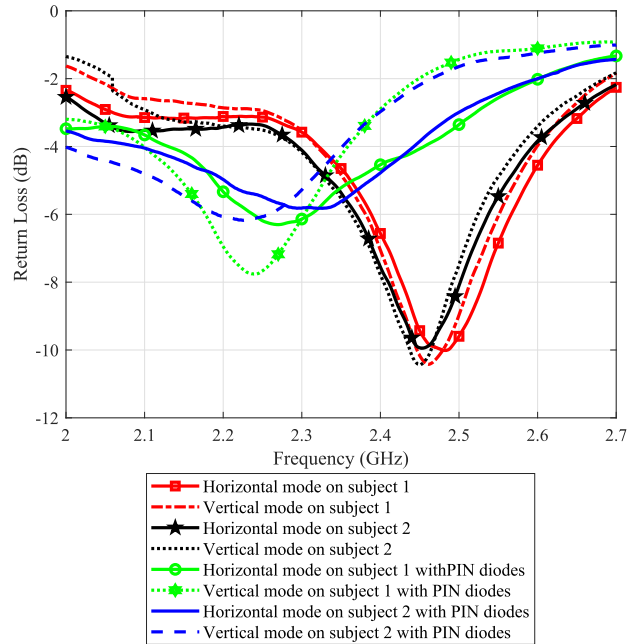


**FIGURE 8.** Measured frequency responses on two different human subjects with a mean of  $2.36$  GHz and a standard deviation of  $0.1$  GHz.

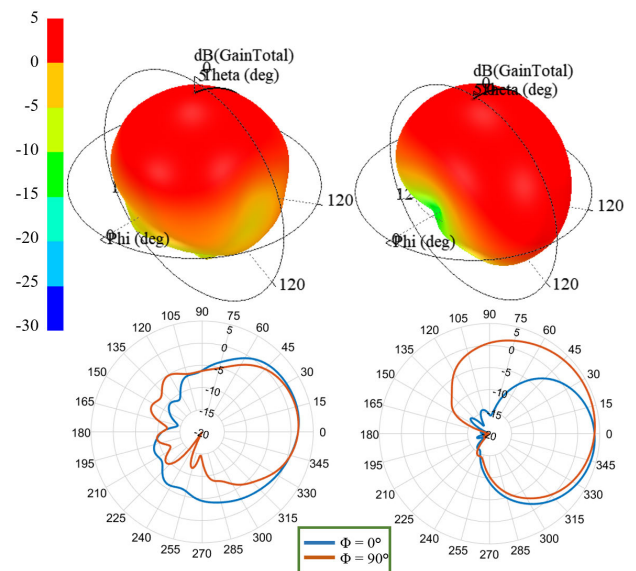


**FIGURE 9.** Simulated 3D radiation patterns and the corresponding 2D cross sections at  $\phi = 0^\circ$  and  $\phi = 90^\circ$  of the horizontal (left) and vertical (right) mode on the ANSYS human body phantom with maximum gains of  $2.3$  dBi and  $4.3$  dBi, respectively.

The measurements on human subjects have been conducted using prototypes that are realized using artificial switches and PIN diodes, NXP BAP 64-03. Fig. 8 shows the measured return loss on two different human subjects. It can be observed that the center frequency does not change for different subjects whereas the magnitude of the reflection coefficient changes in the order of 1 dB. This observation supports our initial assumption of slot antennas being more suitable for wearable applications due to their magnetic nature. When the artificial switches are replaced with PIN diodes,

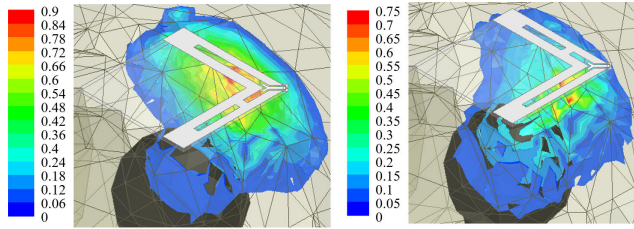


**FIGURE 10. Simulated SAR of the horizontal and vertical mode with maximum values less than 0.95 W/kg and 0.8 W/kg, respectively.**

we can observe that the effective slot length is greater due to the imperfect shorting; hence, the center frequency is shifted by 200 MHz. This effect should be taken into consideration during implementation.

Fig. 9 shows the simulated radiation patterns on the numeric head model along with the corresponding 2D cross sections at  $\phi = 0^\circ$  and  $\phi = 90^\circ$ . It can be seen that the pattern in each mode has become directional with the effect of the phantom. The maximum gain is determined to be 2.3 dBi for the horizontal mode and 4.3 dBi for the vertical mode. The radiation efficiency is 41% for the horizontal mode and 56% for the vertical mode. The horizontal mode couples more to the human head which explains the reason why the radiation efficiency is lower. This effect can be observed in the Specific Absorption Rate (SAR) simulations as well. The SAR of the antenna is simulated for both of the operation modes and the results are shown in Fig. 10. The maximum SAR is determined to be less than 0.95 W/kg for the horizontal mode and 0.8 W/kg for the vertical mode. Both values are well below the limit 2 W/kg specified in the European Standards.

The reconfiguration is intended to be used for antenna selection which can be translated into diversity gain. A simple selection algorithm can be used where one of the two modes can be selected according to the power of the received signal at each mode. The selection can be activated if the received signal drops below a certain threshold to justify the trade-off between the power loss due to RF retransmissions in case of an unreliable link and the power loss due to switching. An established way to prove that different modes will provide different received power levels is to check whether the envelope correlation between two modes is low. Here in the case where the antenna is in air, the envelope correlation,  $\rho_e$ , calculated using (6) is lower than 0.1, where  $\vec{F}_1(\theta, \phi)$  and  $\vec{F}_2(\theta, \phi)$  are the simulated radiation patterns and  $\Omega$  is the solid angle.

$$\rho_e = \frac{|\int_{4\pi} \int [\vec{F}_1(\theta, \phi) \cdot \vec{F}_2(\theta, \phi)] d\Omega|^2}{\int_{4\pi} \int |\vec{F}_1(\theta, \phi)|^2 d\Omega \int_{4\pi} \int |\vec{F}_2(\theta, \phi)|^2 d\Omega} \quad (6)$$

**V. CONCLUSION**

A novel pattern reconfigurable wearable slot antenna operating in the 2.4 GHz ISM band is presented. The antenna is fed by a CPW and switched between two operation modes leading to two different radiation patterns. Glass is used as the substrate of the antenna. The design is simulated and measured in air, on numerical and physical phantoms and

human subjects. It is verified that the antenna exhibits a good impedance matching and operates in the desired band with a maximum gain greater than 1.5 dBi and efficiency greater than 40% in all different cases. It is also shown that the SAR values are below the limit specified in the European Standards. The presented antenna is shown to perform the reconfiguration using PIN diodes and is a promising design for wearable applications. In the future, the authors aim to operate the antenna in a third mode in order to collect data from a contact lens.

**REFERENCES**

- [1] S. Shah, A. Ren, D. Fan, Z. Zhang, N. Zhao, X. Yang, M. Luo, W. Wang, F. Hu, M. Rehman, O. Badarneh, and Q. Abbasi, "Internet of Things for sensing: A case study in the healthcare system," *Appl. Sci.*, vol. 8, no. 4, p. 508, Mar. 2018.
- [2] M. El Abbasi and K. Kabalan, "Revolutionizing the development of wearable antennas," in *Proc. Int. Workshop Antenna Technol. (iWAT)*, Mar. 2019, pp. 54–57.
- [3] K. N. Paracha, S. K. A. Rahim, P. J. Soh, and M. Khalily, "Wearable antennas: A review of materials, structures, and innovative features for autonomous communication and sensing," *IEEE Access*, vol. 7, pp. 56694–56712, 2019.
- [4] S. Dumanli, "On-body antenna with reconfigurable radiation pattern," in *IEEE MTT-S Int. Microw. Symp. Dig. Ser. RF Wireless Technol. Biomed. Healthcare Appl. (IMWS-Bio)*, Dec. 2014, pp. 1–3.
- [5] S. P. Pinapati, S. J. Chen, D. Ranasinghe, and C. Fumeaux, "Detuning effects of wearable patch antennas," in *Proc. IEEE Asia Pacific Microw. Conf. (APMC)*, Nov. 2017, pp. 162–165.
- [6] S. J. Chen, D. C. Ranasinghe, and C. Fumeaux, "A robust snap-on button solution for reconfigurable wearable textile antennas," *IEEE Trans. Antennas Propag.*, vol. 66, no. 9, pp. 4541–4551, Sep. 2018.
- [7] C. G. Christodoulou, Y. Tawk, S. A. Lane, and S. R. Erwin, "Reconfigurable antennas for wireless and space applications," *Proc. IEEE*, vol. 100, no. 7, pp. 2250–2261, Jul. 2012.
- [8] J. Costantine, Y. Tawk, S. E. Barbin, and C. G. Christodoulou, "Reconfigurable antennas: Design and applications," *Proc. IEEE*, vol. 103, no. 3, pp. 424–437, Mar. 2015.
- [9] S. M. Saeed, C. A. Balanis, C. R. Birtcher, A. C. Durgun, and H. N. Shaman, "Wearable flexible reconfigurable antenna integrated with artificial magnetic conductor," *IEEE Antennas Wireless Propag. Lett.*, vol. 16, pp. 2396–2399, 2017.
- [10] R. B. V. B. Simorangkir, Y. Yang, K. P. Esselle, and Y. Diao, "A varactor-tuned frequency-reconfigurable fabric antenna embedded in polymer: Assessment of suitability for wearable applications," in *IEEE MTT-S Int. Microw. Symp. Dig.*, Jun. 2017, pp. 204–207.
- [11] S. F. Jilani and A. Alomainy, "An inkjet-printed MMW frequency-reconfigurable antenna on a flexible PET substrate for 5G wireless systems," in *Proc. Loughborough Antennas Propag. Conf. (LAPC)*, 2017, pp. 1–3.
- [12] S. F. Jilani, B. Greinke, Y. Hao, and A. Alomainy, "Flexible millimetre-wave frequency reconfigurable antenna for wearable applications in 5G networks," in *Proc. URSI Int. Symp. Electromagn. Theory (EMTS)*, Aug. 2016, pp. 846–848.
- [13] T. Sabapathy, M. A. Bashah, M. Jusoh, P. J. Soh, and M. R. Kamarudin, "Frequency reconfigurable rectangular antenna with t-slotted feed line," in *Proc. Int. Conf. Radar, Antenna, Microw., Electron., Telecommun. (ICRAMET)*, Oct. 2016, pp. 81–84.
- [14] A. Javed, B. Bhellar, and F. A. Tahir, "Reconfigurable body worn antenna for Bluetooth and WiMAX," in *Proc. 12th Int. Bhurban Conf. Appl. Sci. Technol. (IBCAST)*, Jan. 2015, pp. 571–573.
- [15] H. Lee and J. Choi, "A polarization reconfigurable textile patch antenna for wearable IoT applications," in *Proc. Int. Symp. Antennas Propag. (ISAP)*, Oct. 2017, pp. 1–2.
- [16] P.-Y. Qin, A. R. Weily, Y. J. Guo, and C.-H. Liang, "Polarization reconfigurable U-Slot patch antenna," *IEEE Trans. Antennas Propag.*, vol. 58, no. 10, pp. 3383–3388, Oct. 2010.
- [17] Y. Li, Z. Zhang, W. Chen, Z. Feng, and M. F. Iskander, "A dual-polarization slot antenna using a compact CPW feeding structure," *IEEE Antennas Wireless Propag. Lett.*, vol. 9, pp. 191–194, 2010.

- [18] Y. Li, Z. Zhang, W. Chen, and Z. Feng, "Polarization reconfigurable slot antenna with a novel compact CPW-to-slotline transition for WLAN application," *IEEE Antennas Wireless Propag. Lett.*, vol. 9, pp. 252–255, 2010.
- [19] X. Tong, C. Liu, X. Liu, H. Guo, and X. Yang, "Switchable ON-/OFF-body antenna for 2.45 GHz WBAN applications," *IEEE Trans. Antennas Propag.*, vol. 66, no. 2, pp. 967–971, Feb. 2018.
- [20] P.-Y. Qin, Y. J. Guo, A. R. Weily, and C.-H. Liang, "A pattern reconfigurable U-slot antenna and its applications in MIMO systems," *IEEE Trans. Antennas Propag.*, vol. 60, no. 2, pp. 516–528, Feb. 2012.
- [21] C.-K. Chang, W.-R. Lin, Y.-Y. Lin, and W.-J. Liao, "Diversity antenna design for compact devices of IoT uses," in *Proc. IEEE Int. Workshop Electromagn., Appl. Student Innov. Competition (iWEM)*, May 2016, pp. 1–3.
- [22] I. Lim and S. Lim, "Monopole-like and boresight pattern reconfigurable antenna," *IEEE Trans. Antennas Propag.*, vol. 61, no. 12, pp. 5854–5859, Dec. 2013.
- [23] R. Masood, C. Person, and R. Sauleau, "A dual-mode, dual-port pattern diversity antenna for 2.45-GHz WBAN," *IEEE Antennas Wireless Propag. Lett.*, vol. 16, pp. 1064–1067, 2017.
- [24] M. Li, S.-Q. Xiao, and B.-Z. Wang, "Pattern-reconfigurable antenna for on-body communication," in *IEEE MTT-S Int. Microw. Symp. Dig. Workshop Ser. RF Wireless Technol. Biomed. Healthcare Appl. (IMWS-BIO)*, Dec. 2013, pp. 1–3.
- [25] S. Dumanli, "A radiation pattern diversity antenna operating at the 2.4 GHz ISM band," in *Proc. IEEE Radio Wireless Symp. (RWS)*, Jan. 2015, pp. 102–104.
- [26] A. Narbudowicz, M. J. Ammann, and D. Heberling, "Switchless reconfigurable antenna with 360° steering," *IEEE Antennas Wireless Propag. Lett.*, vol. 15, pp. 1689–1692, 2016.
- [27] Y. Li, Z. Zhang, J. Zheng, Z. Feng, and M. F. Iskander, "Experimental analysis of a wideband pattern diversity antenna with compact reconfigurable CPW-to-slotline transition feed," *IEEE Trans. Antennas Propag.*, vol. 59, no. 11, pp. 4222–4228, Nov. 2011.
- [28] A. da Conceição Andrade, I. P. Fonseca, S. F. Jilani, and A. Alomainy, "Reconfigurable textile-based ultra-wideband antenna for wearable applications," in *Proc. 10th Eur. Conf. Antennas Propag. (EuCAP)*, Apr. 2016, pp. 1–4.
- [29] H. A. Majid, M. K. A. Rahim, M. R. Hamid, and M. F. Ismail, "Frequency and pattern reconfigurable slot antenna," *IEEE Trans. Antennas Propag.*, vol. 62, no. 10, pp. 5339–5343, Oct. 2014.
- [30] S. J. Chen, D. C. Ranasinghe, and C. Fumeaux, "A polarization/frequency interchangeable patch for a modular wearable textile antenna," in *Proc. 11th Eur. Conf. Antennas Propag. (EUCAP)*, Mar. 2017, pp. 2483–2486.
- [31] M. I. Jais, M. F. Jamlos, M. Jusoh, T. Sabapathy, and M. R. Kamarudin, "2.45 GHz beam-steering textile antenna for WBAN application," in *Proc. IEEE Antennas Propag. Soc. Int. Symp. (APSURSI)*, Jul. 2013, pp. 200–201.
- [32] S.-J. Ha and C. W. Jung, "Reconfigurable beam steering using a microstrip patch antenna with a U-Slot for wearable fabric applications," *IEEE Antennas Wireless Propag. Lett.*, vol. 10, pp. 1228–1231, 2011.
- [33] S. Kang and C. W. Jung, "Wearable fabric antenna on upper arm for MedRadio band applications with reconfigurable beam capability," *Electron. Lett.*, vol. 51, no. 17, pp. 1314–1316, Aug. 2015.
- [34] S. Yan and G. A. E. Vandenbosch, "Wearable pattern reconfigurable patch antenna," in *Proc. IEEE Int. Symp. Antennas Propag. (APSURSI)*, Jun. 2016, pp. 1665–1666.
- [35] E. Cil and S. Dumanli, "The design of a pattern reconfigurable antenna suitable for smart glasses," in *Proc. IEEE 30th Int. Symp. Pers., Indoor Mobile Radio Commun. (PIMRC Workshops)*, Sep. 2019, pp. 1–4.
- [36] C. A. Balanis, *Antenna Theory: Analysis and Design*. Hoboken, NJ, USA: Wiley, 2016.
- [37] A. W. Rudge and K. Milne, *The Handbook of Antenna Design*, vol. 16. Edison, NJ, USA: IET, 1982.
- [38] J. D. Kraus and R. J. Marhefka, *Antennas For All Applications*. New York, NY, USA: McGraw-Hill, 2002.
- [39] (Oct. 2019). *Ansys HFSS*. [Online]. Available: <http://www.ansys.com/products/electronics/ansys-hfss>
- [40] (Oct. 2019). *Voltera V-One*. [Online]. Available: <https://www.voltera.io/>
- [41] A. T. Mobashsher and A. M. Abbosh, "Three-dimensional human head phantom with realistic electrical properties and anatomy," *IEEE Antennas Wireless Propag. Lett.*, vol. 13, pp. 1401–1404, 2014.
- [42] (Feb. 2020). *IT'IS Foundation Dielectric Properties Table*. [Online]. Available: <https://itis.swiss/virtual-population/tissue-properties/database/dielectric-properties/>
- [43] F. M. Ghannouchi and R. G. Bosisio, "Measurement of microwave permittivity using a six-port reflectometer with an open-ended coaxial line," *IEEE Trans. Instrum. Meas.*, vol. 38, no. 2, pp. 505–508, Apr. 1989.



**ERDEM CIL** received the B.Sc. degree in electronics and communication engineering from Istanbul Technical University, Istanbul, Turkey, in 2017. He is currently pursuing the M.Sc. degree with the Electronics Department, Bogazici University, Istanbul.

He is also a Research Assistant with the Electronics Department, Bogazici University. His current research interests include reconfigurable antenna design for flexible and wearable devices.



**SEMA DUMANLI** (Member, IEEE) received the B.Sc. degree in electrical and electronic engineering from Orta Dogu Teknik Universitesi, Ankara, Turkey, in 2006, and the Ph.D. degree from the University of Bristol, Bristol, U.K., in 2010.

She was with Toshiba Research Europe, Bristol, as a Research Engineer and a Senior Research Engineer, from 2010 to 2017. She is currently an Assistant Professor with Bogazici University, Istanbul, Turkey. Her current research interests

include antenna design for body area networks, implantable and wearable devices, e-health, and multi-in-multi-out communications.

...